Morsy *et al.*
Journal of Engineering and Applied Science (2022) 69:62
https://doi.org/10.1186/s44147-022-00102-7

Journal of Engineering and Applied Science

RESEARCH Open Access

Effect of welding parameters on the mechanical and metallurgical properties of armor steel weldment

M. A. Morsy[1], Sabry M. Abdel Aziz[2*], Khaled Abdelwahed[3] and Sabreen A. Abdelwahab[2]

*Correspondence: eng.sabrimoussa1976@gmail.com

[1] Welding and NDT Department, CMRDI, Cairo, Egypt
[2] Department of Production Technology, Faculty of Technology and Education, Helwan University, Cairo, Egypt
[3] Department of Automotive and Tractors Technology, Faculty of Technology and Education, Helwan University, Cairo, Egypt

Abstract

The effect of welding parameters on the mechanical and metallurgical properties of armor steel weldment was studied using gas tungsten arc welding process with two filler wires: carbon steel and austenitic stainless-steel filler wires (AWS A5.18 ER 70S-6 and AWS A5.9 ER 307, respectively). The joint configurations were mainly single V and single bevel grooves. Using both AWS A5.18 ER70S-6 carbon steel filler wire and AWS A5.9 ER307, austenitic filler wire for the two joints passed the required tensile strength by the military standard. The joints successfully regained the base metal hardness at a distance of less than 15 mm. The ultimate tensile strength of the joints welded in a single bevel groove is 906 MPa which is higher than the joints welded using a single V groove is 865 MPa. This could be attributed to the increase in dilution percentage with the single bevel joints. Both single V joint and single bevel joints passed the required Charpy V-notch impact test whether using both carbon and stainless-steel wires. The effect of heat input and cooling rate on the mechanical and microstructure of welded joints was studied. The reduction of heat input caused a narrow HAZ with a small reduction in its hardness values with much reduction in the width of softening microstructure zone. SEM observations show that the base metal has a martensitic structure, but the weld metal microstructures depend on the filler: carbon steel or austenitic steel types. Using a single bevel groove with an austenitic steel filler metal, the weld metal shows a martensitic/austenitic microstructure by SEM observation, and this was verified by the Schaeffler diagram which showed a high dilution percentage (about 35% dilution). This resulted in a significant increase in joint strength and a higher weld metal impact resistance.

Keywords: Gas tungsten arc welding (GTAW) process, MIL A 46100 armor steel joints, Heat-affected zone softening, Weld thermal cycle, Heat input, Microstructural characterization, SEM observation, Hardness distribution, Tensile test, Impact test

Introduction

Although there are many ballistic protection applications that use nonferrous or even nonmetallic armor, armor steels are still the leading material in applications where impact and explosion protection is critical [1–4]. The ballistic performance of steel

Springer Open

© The Author(s) 2022. **Open Access** This article is licensed under a Creative Commons Attribution 4.0 International License, which permits use, sharing, adaptation, distribution and reproduction in any medium or format, as long as you give appropriate credit to the original author(s) and the source, provide a link to the Creative Commons licence, and indicate if changes were made. The images or other third party material in this article are included in the article's Creative Commons licence, unless indicated otherwise in a credit line to the material. If material is not included in the article's Creative Commons licence and your intended use is not permitted by statutory regulation or exceeds the permitted use, you will need to obtain permission directly from the copyright holder. To view a copy of this licence, visit http://creativecommons.org/licenses/by/4.0/. The Creative Commons Public Domain Dedication waiver (http://creativecommons.org/publicdomain/zero/1.0/) applies to the data made available in this article, unless otherwise stated in a credit line to the data.

depends essentially on its mechanical behavior under the very high load rate experienced at ballistic speeds [5, 6].

Armor steels, sometimes called ballistic steels, are classified in the AWS standards and in military standards [7, 8]. A combination between the standards is used to classify and identify the metal and methods to process it, in the AWS under the category of quenched and tempered [7]. Therefore, these steels have high strength, hardness, and good toughness where these materials acquired strength up to 1000 MPa. Most of the higher processed materials that exceed this range are identified in the military standard MIL-St A46100 [8]. The issue with the armor steel is that it reaches very high hardness (around 500 HV) and tensile strength (around 1650 MPa) using complicated processing called thermomechanical controlled processing (TMCP) at high temperatures, including quenched and tempering. This process resulted in the fine grains martensitic structure with ultrahigh strength properties, considering that this makes the steel sensitive to any thermal processing including cutting and welding processes [7, 9].

Armox 500T armor steel plates [4, 6] are used for military applications as well as for civil applications such as the counters for banks, doors, and vehicles for safe people and money transport, and tank body shielding, and police vehicles [4, 6].

Welding of armor steel is a crucial and important task in both military and civil usage of this kind of steel, although mainly classified as HSLA (high-strength low-alloy steel) having a low percentage of alloying elements to improve weldability and meet some challenges in welding, as to reach the military requirements in strength, hardness, and toughness [10–14].

In the heat-affected zone (HAZ), softening occurs when these steels are exposed to high temperatures in welding. This softening leads to degradation in ballistic performance. The degree of softening in the heat-affected zone is depending on the level of temperature rise which in turn is a function of the welding process and heat input [7, 15, 16]. Increased heat input leads to a wider softening of HAZ, and the ballistic performance is inversely proportional to the width of the heat-affected zone softening [12, 15, 16]. Therefore, there is an urgent need to optimize the welding parameters for improving mechanical properties and ballistic performance to meet the military standard [17, 18].

The appropriate filler metals should be selected for the weld of armor steels in order to achieve an optimum combination of strength and toughness in the welded joint. Matching or overmatching should be avoided in order to produce cracking's free joints with improving toughness and ductility [19, 20].

Alkemade S. J [21]. studied the weld cracking of armor steel using a restraint Y-groove joint. He found that increased preheat temperature and heat input resulted in a disappearance of cold cracking in the welded joint. Thus, higher cooling rates encourage the formation of cold cracking in their welded joints [21].

In the previous paper, gas metal arc welding (GMAW) and gas tungsten arc welding (GTAW) were applied to the welding of SEWBOR 500 armor steel of 6 mm thickness. The joint welded with AWS A5.18 ER70S-6 filler metal with MAG welding process has not satisfied hardness width requirements by the military standard [7]. This could be attributed to the low cooling rate associated with this process.

Reddy et al. [22, 23] investigated the ballistic performance of armor steel and its GMAW weldments against 7.62 AP bullet. The weldments were prepared with

different welding speeds and heat inputs. Furthermore, the results revealed that the weldments with greater heat input value show poor ballistic performance [22, 23].

Therefore, the welding parameter should be adjusted to get welded joint without cold cracking (high heat input and apply preheat temperature, i.e., reduce the cooling rate). Also, the reduction of the width of an over-tempered zone by increasing the cooling rate should be adjusted to satisfy the width requirements by the military standards [7, 21]. External factor such as cooling by compressed air at gentle pressure of 6 bars may be introduced after completion of the welding pass to reduce the width of the softening zone.

Military standards demonstrate that the ultimate tensile strength of welded joints should exceed 750 MPa to be succeeded using carbon steel filler metal. However, they should exceed a minimum ultimate tensile strength of 550 MPa using austenitic stainless steel filler metal. The retainment of the base metal hardness value must be achieved at a distance of 16 mm measured from the centerline of the weld metal. The Charpy V-notch impact test results of both weld metal and heat-affected zone are also important [7, 14, 18].

GTAW is preferred because of its better weld properties suited for joining advanced steel plates [24], Through control in welding parameters such as welding voltage, welding current, shielding gas, and the metal flow rate, that controls the penetration of the joint [25, 26].

Always in the study of welded joint properties of steel, the cooling rate is determined in a temperature range between 800 and 500 °C. However, in welding of Armox steel, the cooling rate between 600 and 200 °C is also very important to reflect the phase transformation of the HAZ as investigated by Aleksander and Katarina [27].

Because of the difficulty in performing ballistic tests, the assessment of welding performance will be according to the HAZ thickness. These articles stated [7, 18, 22, 28] that welds with a HAZ width of 16 mm or less withstood the bullets fired thereon, while if the HAZ increases, the performance of the plate will fail, and thus, the hardness distribution and recovery are examined in detail for each sample from the weld metal centerline to the base metal [7, 18, 28].

Requirements of quality for the welding of MIL-A-46100 steel are given by MIL-STD 1185 [28] and SD-X12140 [29] standards. The requirements are divided into three categories: (i) mechanical properties, (ii) weld soundness, and (iii) in-service performance.

Requirements for weld soundness are stated in military standards [28] and in AWS D1.1 [30] and ASME Section IX [31] standards for requirements of a sound weld.

The main aim of the research is to improve armor steel weldment properties using GTAW process by reducing the width of the heat-affected zone to meet the requirements of military codes. Therefore, two types of filler metals will be applied, and also two types of joint configuration will be used. The effect of heat input and cooling rate will be studied in order to optimize the welding conditions leading to improving the performance of welded joints and meeting the requirements of military standards [7, 8, 18]. The results will be discussed on the basis of the mechanical and metallurgical properties of the welded joints.

Methods and experimental procedure

This section describes the used materials and experimental and testing methods.

Materials

The base metal was Armox 500T which is a commercial name for armor sheet metals with a dimension of 200 × 155 × 10 mm. The heat treatment includes austenitizing at 900 °C and then water quenching and followed by tempering at 200 °C [32]. The obtained base metal has high hardness and strength with acceptable toughness. The chemical composition and mechanical properties from the SSAB company specification of base metal are presented in Tables 1 and 2.

Filler metal types and their mechanical properties

Two filler metals are used with the GTAW process: one is a carbon steel AWS A5.18 ER70S-6, and the other is an austenitic type AWS A 5.9 ER 307. The selection was based on the results obtained in previous literature by [7, 16, 22, 33] and filler metal manufacturers' specifications [19, 34, 35] and requirements for the welding of armor steel according to MIL-STD 1185 standards [28]. Using austenitic filler metal is an advantage to decrease the susceptibility to cold cracking [16, 33]. The welder tries to apply the lowest level filler wire welding current in order to reduce the deterioration of HAZ microstructure as a result of softening [6, 7, 16, 18, 22]. The chemical compositions and mechanical properties of all deposited weld metals are shown in Tables 3 and 4.

Welding joints fabrication and thermocouple location

Two different weld groove shapes namely single V and single bevel grooves were fabricated using machine CNC high-speed wire cut EDM (model FW 2U series — Switzerland). An

Table 1 Chemical compositions of the Armox 500T steel plate (SSAB company specification), wt.%

Nominal composition %											
Elements	**C Max**	**Si Max**	**Mn Max**	**P Max**	**S Max**	**Cr Max**	**Ni Max**	**Mo Max**	**B Max**	**CE**	**Fe**
Standard	0.32	0.4	1.2	0.010	0.003	1.0	1.8	0.7	0.005	0.67	Bal

Table 2 The mechanical properties of the Armox 500T steel plate (SSAB company specification)

Hardness (HBW)	**Yield strength, min (MPa)**	**Tensile strength (MPa)**	**Elongation, min (%)**	**Charpy V-notch impact test specimen, min (10 × 10 × 55 mm) at −40 °C**
480–540	1250	1450–1750	8	32 (J)

Table 3 The chemical composition of all weld metals of filler wires, wt. %

Elements	**C**	**Si**	**Mn**	**P**	**S**	**Cr**	**Ni**	**Mo**	**V**	**Fe**
AWS A 5.9 ER 307	0.09	0.9	7	0.001	0.002	19	8.5	0.13	0.03	Bal
AWS A 5.18 ER 70S-6	0.07	0.8	1.45	0.002	0.003	0.025	0.05	0.002	0.012	Bal

Table 4 Mechanical properties of all weld metals of filler wires [34]

Weld metal type	Yield strength (MPa)	Tensile strength (MPa)	Elongation (%)	Impact tests	
				+20 °C	−40 °C
AWS A5.18 ER70S-6	440	540	28	120	50
AWS A5.9 ER 307	430	620	42	120	110

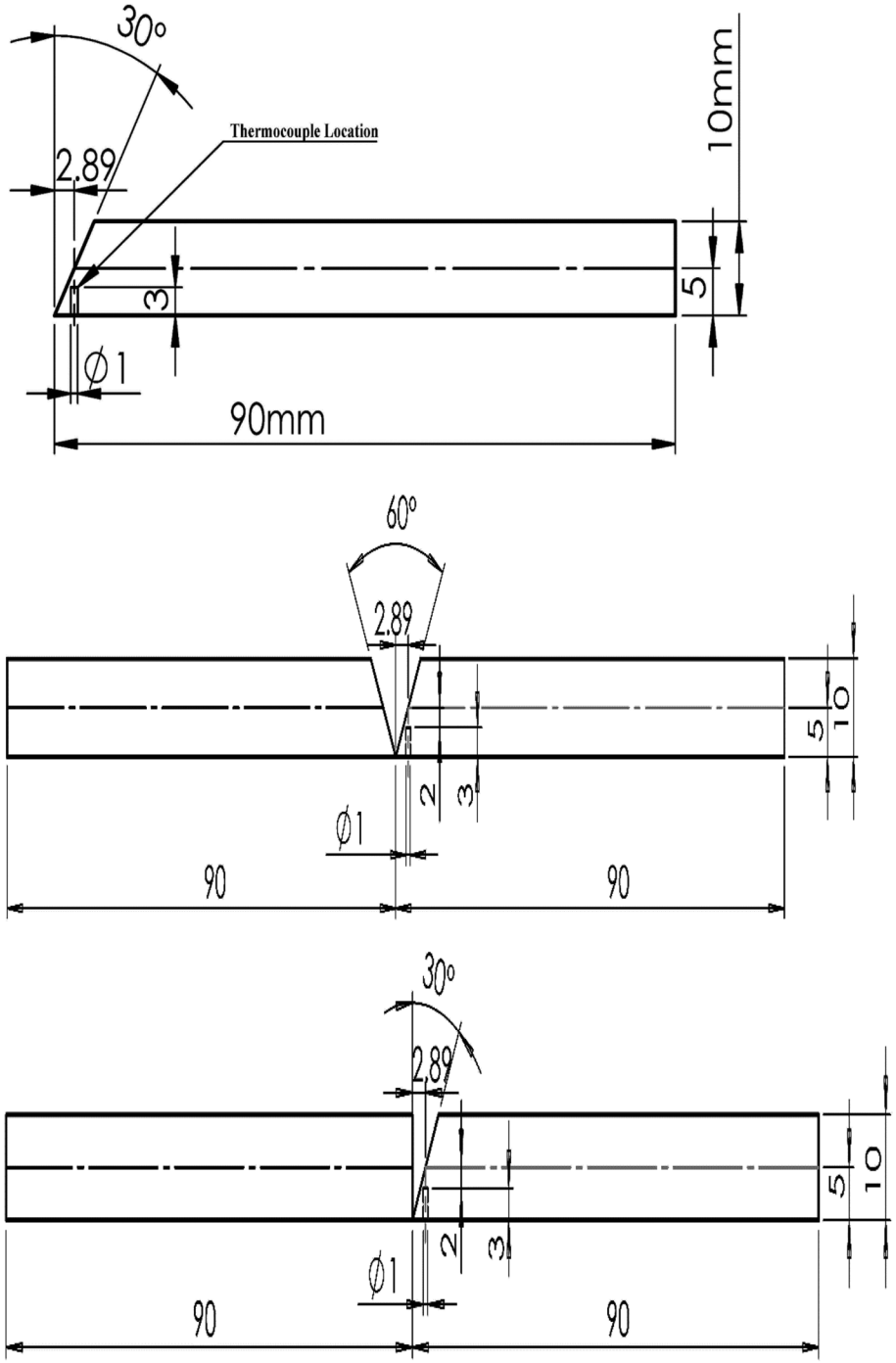

Fig. 1 Schematic drawing of edge preparation showing thermocouple location

Table 5 Welding procedure parameters

Sample	Number of passes	Welding current (A)	Arc voltage (V)	Travel speed (mm/min)	Heat input (kJ/mm)[a]
Single V/AWS A 5.18 ER 70S-6 without cooling	12	135	13	49.76	1.1
Single bevel/AWS A 5.18 ER70S-6 without cooling	9	135	13	47.61	1.1
Single V/AWS A 5.9 ER 307 without cooling	9	130	13	28.17	1.7
Single bevel/AWS A 5.9 ER 307 without cooling	9	130	13	31.25	1.6
Single V/AWS A 5.18 ER 70S-6 with cooling	4	110	13.2	33.33	1.4
Single bevel/AWS A 5.18 ER 70S-6 with cooling	4	110	13.2	35.04	1.1
Single V/AWS A 5.9 ER 307 with cooling	4	110	13.2	33.51	1.3
Single bevel/AWS A 5.9 ER307 with cooling	4	110	13.2	31.26	1.4

Table 6 Welding procedure conditions

Base metals	Armox 500T			
Thickness of plate	10 mm			
Welding process type	GTAW			
Welding machine type	Fronius Magic Wave 3000			
Filler metal type	AWS A5.18 ER 70S-6	AWS A 5.9 ER 307	AWS A 5.18 ER 70S-6	AWS A 5.9 ER 307
Joint type and angle	Single V (60°) and single bevel (30°)			
Filler wire diameter (mm)	2.4	1.6	2.4	1.6
Gas (%)	100% argon			
Gas flow rate l/min	10 l/min	10 l/min, back shield 8 l/min	10 l/min	10 l/min, back shield 8 l/min
Welding method	Continuous		Not continuous	
Cooling method	Without cooling (left at ambient temperature after completion of the whole welding)		With using compressed air (6 bars) in the cooling after each pass up to 100 °C	

impermeable hole with a diameter of 1 mm was carried out in the centerline of specimens at a distance of 2.89 mm from the root edge of the groove as shown in Fig. 1 with a depth of 3 mm from the bottom of the sample, using CNC electrical discharge-forming machine (model DM 450 series — China). A K-type thermocouple is inserted in the hole to measure the temperature change in the heat-affected zone (HAZ).

Welding process and shielding gas

The GTAW process is applied using a welding machine type (Fronius Magic Wave 3000). The welding parameters and conditions are listed in Tables 5 and 6, respectively. A 100% argon gas is applied in the case of using AWS A 5.9 ER 307 austenitic stainless steel filler metal with a flow rate of 10 l/min. Argon back shielding is applied in the case of using AWS A5.9 ER307 filler metal with a flow rate of 8 l/min. And also, a 100% argon gas is used in the case of AWS A 5.18 ER 70S-6 carbon steel filler metal with a flow rate of 10 l/min. Figure 2

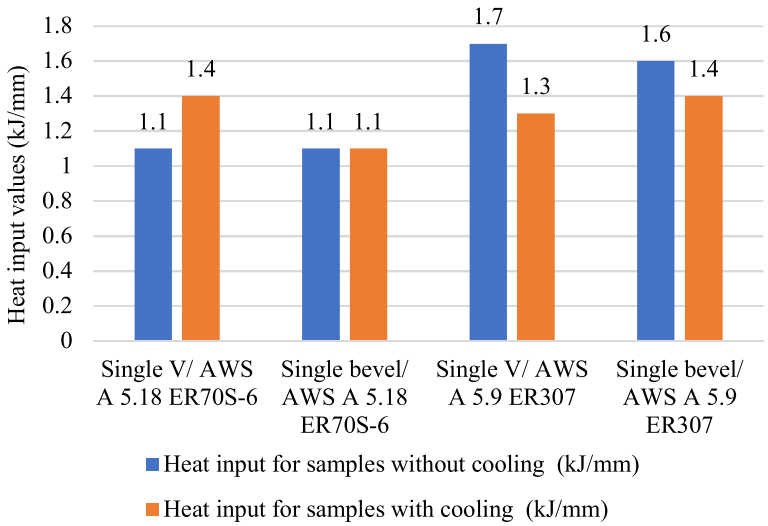

Fig. 2 Heat input values of all specimens

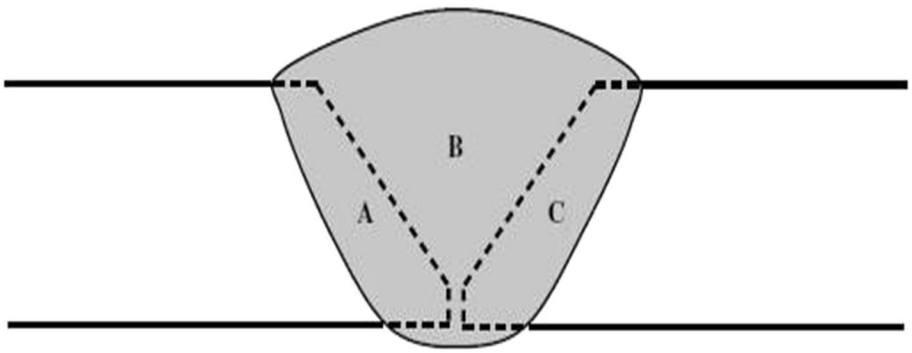

Fig. 3 Calculation of percent dilution

represents the heat inputs at different welding conditions. Cooling is applied immediately after completion of each pass by using compressed air with a pressure of 6 bars.

*The heat input is determined using Eq. (1)

$$Hi = \mu \frac{\boldsymbol{V\ I\ 60}}{\boldsymbol{S\ 1000}}\ (\text{kJ/mm}) \tag{1}$$

Hi: Heat input (kJ/mm)
V: Arc voltage (Volts)
I: Current (Amperage)
μ: Thermal efficiency ($GTAW = 0.6$)
S: Travel speed (mm/min)

Metallurgical properties of the joints

An optical emission spectrometry equipment is used to determine the chemical compositions of base metal and weld metals. Etching using a 2% nital solution was used

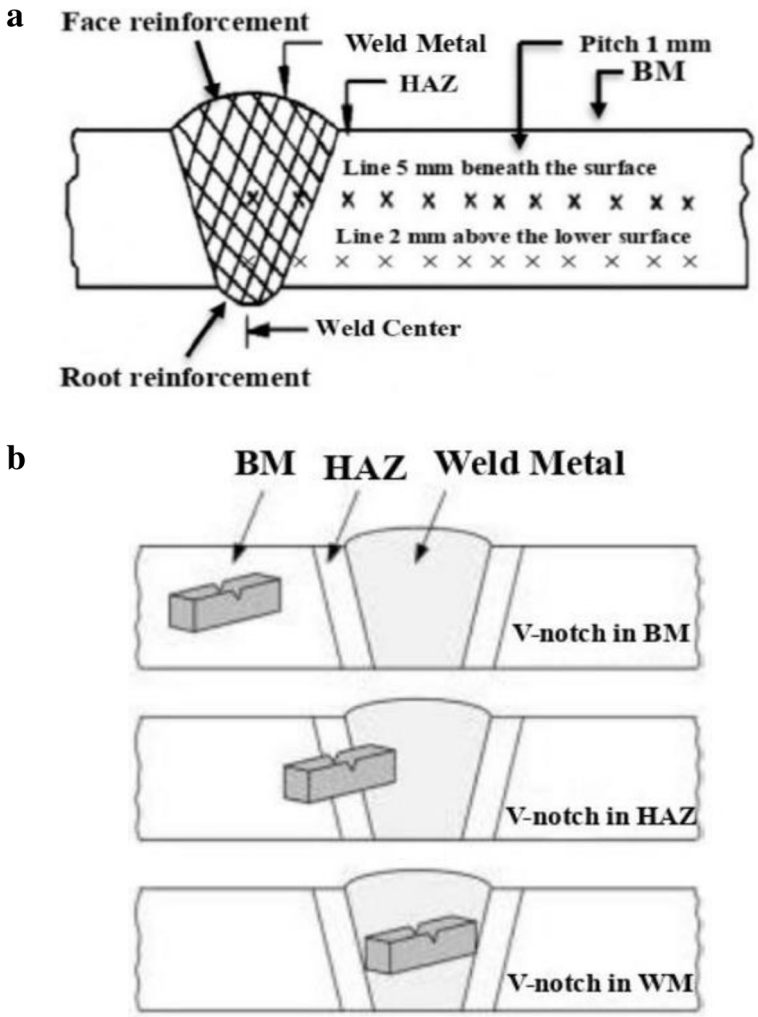

Fig. 4 **a** Location of hardness distribution measurements of the welded specimen [16]. **b** Location of V-notch of the welded specimen for impact test [36]

to reveal the martensitic and ferritic structures. However, 10% oxalic acid was used to reveal the austenitic structure. A stereoscope is used to show the macrostructure of welded joints. Microstructure characteristics were carried out by using a light optical microscope (OLYMPUS MODEL PMG3 \-F3). SEM observations were carried out by using a machine model (QUANTA FEG 250). The dilution percentage was calculated using Eq. (2) illustrated in Fig. 3 [36].

$$\text{Dilution } (\%) = \frac{A + C}{A + B + C} * 100 \tag{2}$$

Table 7 Chemical compositions of the Armox 500T steel plate, wt. %

Elements	C	Si	Mn	P	S	Cr	Ni	Mo	B	CE	Fe
Company specification	0.32 Max	0.4 Max	1.2 Max	0.010 Max	0.003 Max	1.0 Max	1.8 Max	0.7 Max	0.005 Max	0.67 Max	Bal
Actual analysis	0.154	0.2	0.88	0.009	0.003	0.5	0.89	0.36	0.001	0.56	Bal

Table 8 The mechanical properties of the Armox 500T steel plate

Hardness (HV)	Yield strength (MPa)	Tensile strength (MPa)	Elongation (%)	Charpy V-notch impact test specimen (10 × 10 × 55 mm) at −40 °C
450	1250	1650	8.9	34 (J)

Destructive and nondestructive testing of welded joints

A dye penetrant test (PT) was applied to the welded joints to observe the surface defects. However, a magnetic particle test (MT) was applied to the joints welded with AWS A5.18 70S-6 only to observe the existence of surface defects. A radiographic test (RT) was applied to observe the existence of internal welding defects. Hardness distribution measurements were done using a Vickers hardness testing machine (DVK-2 Tokyo Japan) with a 20 kg load for 70 s. The hardness profile through weld metal, HAZ, and the base metal will be determined with a pitch of measurement position of 1 mm as shown in Fig. 4a; the test has been carried out according to ASTM standards [37]. Transverse tensile tests have been carried out using a tensile machine (universal testing machine WDW-300 China). The test has been carried out according to ASTM A370-12 [38], using two specimens. Charpy V-notch impact test was done using a Charpy V-notch impact testing machine using a low-temperature chamber at −40 °C and also at room temperature. Charpy impact tests in the weld metal and HAZ were performed as shown in Fig. 4b according to ASTM E23-12 c standard [39, 40]. Five readings were taken in each location.

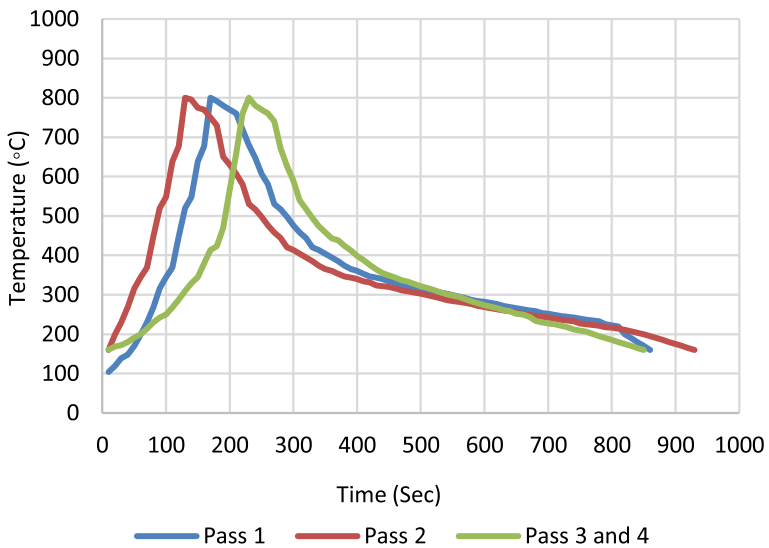

Fig. 5 Temperature cycle for single V using AWS A 5.9 ER307 without cooling

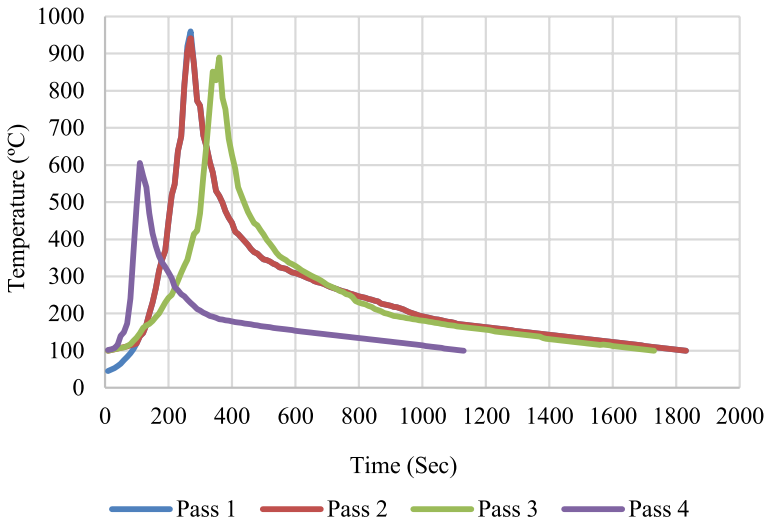

Fig. 6 Temperature cycle for single V using AWS A5.18 ER70S-6 with cooling

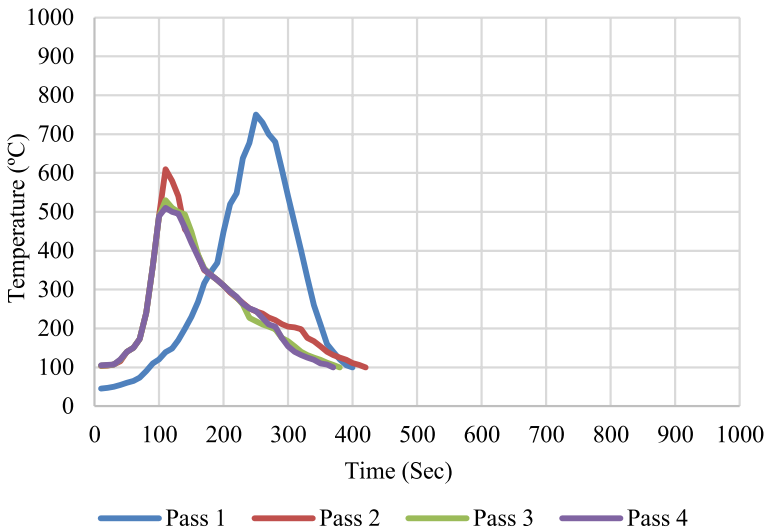

Fig. 7 Temperature cycle for single bevel using AWS A5.18 ER70S-6 with cooling

Results and discussion

Base metal composition and their mechanical properties

The chemical analysis of base metal from SSAB company specification and actual analysis for base metal are presented in Table 7. The mechanical properties are shown in Table 8.

Effect of cooling rate of welded joints

As mentioned in "Introduction", the cooling rate between 600 and 200 °C is also very important to reflect the phase transformation of the HAZ as investigated by Aleksander and Katarina [27].

Figure 5 shows the cooling rate of welded samples without using compressed air after completion of welding. The cooling time (Δt 8/5) of the first pass is 35 s, and its cooling

rate (Δt 8/5) is 8.5 °C/s. The cooling rate (Δt 8/5) of the second, the third, and the fourth passes is 10 °C/s. The cooling time (Δt 6/2) of the first pass is 235 s, and its cooling rate (Δt 6/2) is 1.72 °C/s. The cooling rate (Δt 6/2) of the second, the third, and the fourth passes is 1.63 °C/s, 1.73 °C/s, and 1.73 °C/s, respectively. Without the application of cooling, the hardness distribution shows a value of 389 HV at a distance of 17 mm from the center of weld metal. This did not satisfy the requirements of military standards [7, 8, 14, 18] (Fig. 17, "Hardness distribution results"). The same results were obtained with Morsy Amin Morsy et al. [7] in welding with the GMAW process using ferritic and austenitic wires.

Visual, PT, and RT show crack-free welded joints without any defects.

Figure 6 shows the cooling rate at the HAZ with the application of compressed air immediately after completion of welding. The cooling time (Δt 8/5) of the first pass is 25 s, and its cooling rate (Δt 8/5) is 12 °C/s. The cooling rate (Δt 8/5) of the second and the third passes is 12 °C/s. The cooling time (Δt 6/2) of the first pass is 110 s, and its cooling rate (Δt 6/2) is 3.63 °C/s. The cooling rate (Δt 6/2) of the second, the third, and the fourth passes is 3.53 °C/s, 3.63 °C/s, and 3.43 °C/s, respectively. With the application of cooling, the hardness distribution shows 450 HV at 14 mm from the center of welded metal, which satisfy the requirements of military standards (Fig. 15, "Hardness distribution results").

Visual, MT, and RT testing show crack-free welded joints without any defects. This indicated that the gentle cooling by compressed air after each pass with a pressure of 6 bars did not show any cracks and it is safe. The same results were obtained in the work of Aleksandar Cabrilo et al. [27] using GMAW with AWS A5.9 ER307 without application of compressed air. They left the joint to be cooled in atmospheric air after each pass.

Figure 7 shows the cooling rate at the HAZ with the application of compressed air at the completion of welding. The cooling time (Δt 8/5) of the first pass is 50 s, and its cooling rate (Δt 8/5) is 6 °C/s. The cooling time (Δt 6/2) of the first pass is 100 s, and its cooling rate (Δt 6/2) is 4 °C/s. The cooling rate (Δt 6/2) of the second, the third,

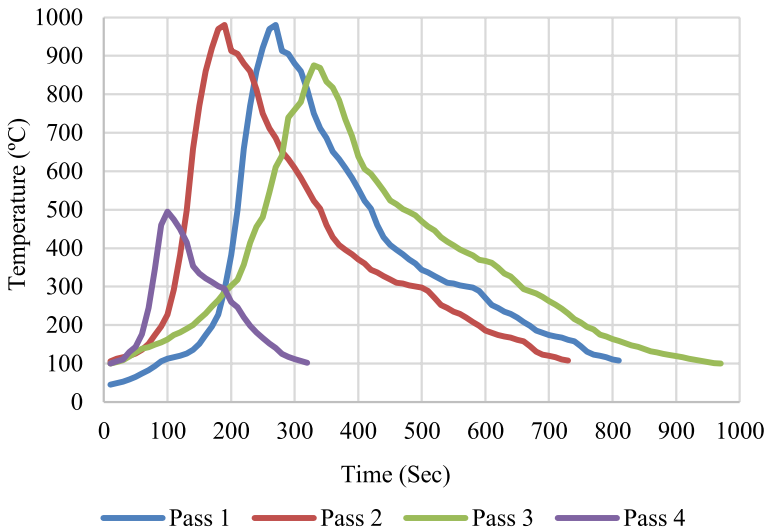

Fig. 8 Temperature cycle for single V using AWS A 5.9 ER 307 with cooling

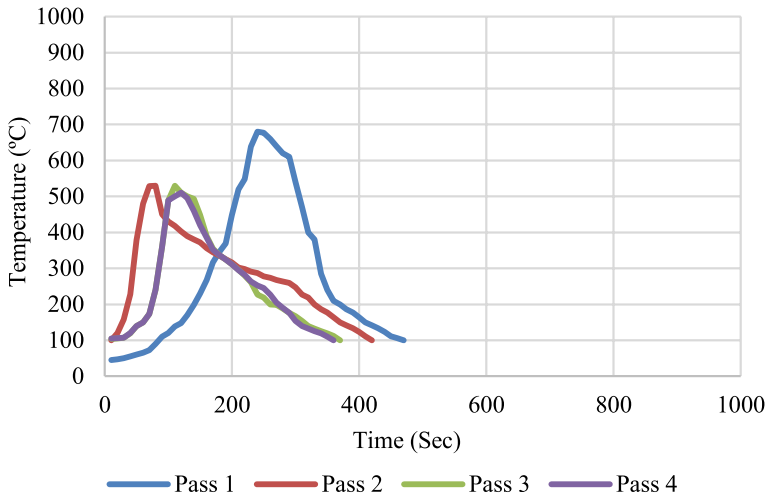

Fig. 9 Temperature cycle for single bevel using AWS A 5.9 ER 307 with cooling

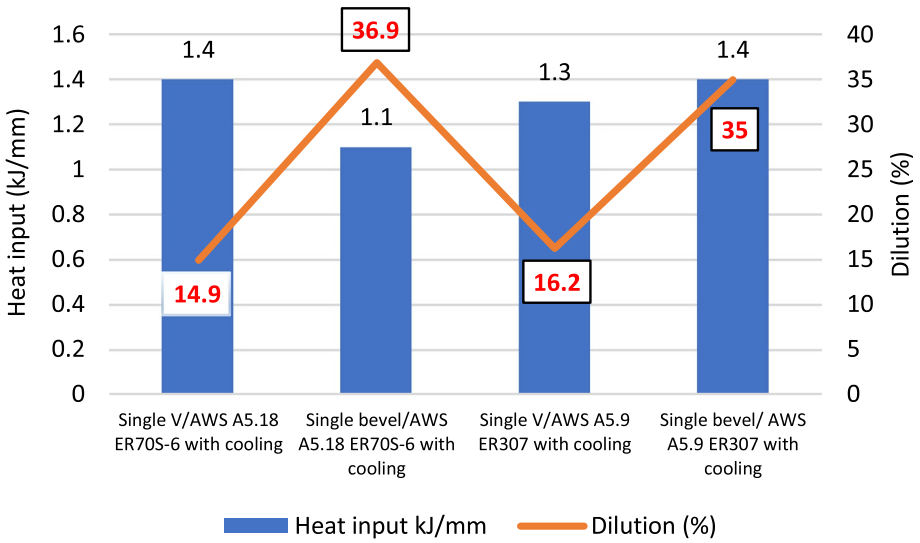

Fig. 10 Effect of joint configuration, heat input, and weld metals on dilution using GTAW process

and the fourth passes is 2.1 °C/s, 3 °C/s, and 2.3 °C/s, respectively. With the application of cooling, the hardness distribution shows a retainment of hardness value at 13 mm from the center of welded metal with a value of 455 HV, i.e., satisfy the requirements of military standards (Fig. 16, "Hardness distribution results").

Visual, MT, and RT testing show crack-free welded joints without any defects. This indicated that the gentle cooling by compressed air after each pass with a pressure of 6 bars did not show any cracks and it is safe.

Figure 8 shows the cooling rate at the HAZ with the application of compressed air at the completion of welding. The cooling time (Δt 8/5) of the first pass is 30 s, and its cooling rate (Δt 8/5) is 10 °C/s. The cooling rate (Δt 8/5) of the second and the third passes is 12 °C/s. The cooling time (Δt 6/2) of the first pass is 120 s, and its cooling rate (Δt 6/2) is 3.3 °C/s. The cooling rate (Δt 6/2) of the second, the third, and the

Table 9 Tensile strength of welded joints

Joint type and filler metal classification	Tensile strength of samples without cooling, MPa	Tensile strength of samples with cooling, MPa	Fracture location	Strength of all weld metal (pure) used, MPa [7, 34]
Single V/AWS A 5.18ER70S-6	780	865	WM	540
Single bevel/AWS A 5.18 ER70S-6	820	890	WM	540
Single V/AWS A 5.9 ER 307	865	893	WM	620
Single bevel/AWS A 5.9 ER 307	892	906	WM	620

fourth passes is 2.35 °C/s, 2.35 °C/s, and 2.5 °C/s, respectively. With the application of cooling, the hardness distribution shows 460 HV hardness value at 15 mm from the center of welded metal, which satisfy the requirements of military standards (Fig. 17, "Hardness distribution results").

Visual, PT, and RT testing show crack-free welded joints without any defects. This indicated that the gentle cooling by compressed air after each pass with a pressure of 6 bars did not show any cracks and it is safe. The same results were obtained in the work of Aleksandar Cabrilo et al. [27] using GMAW with AWS A5.9 ER307 filler wire. They did not apply compressed air; however, they left the joint to be cooled in atmospheric air after each pass.

Figure 9 shows the cooling rate at the HAZ with the application of compressed air at the completion of welding. The cooling time (Δt 8/5) of the first pass is 30 s, and its cooling rate (Δt 8/5) is 10 °C/s. The cooling time (Δt 6/2) of the first pass is 80 s, and its cooling rate (Δt 6/2) is 5 °C/s. The cooling rate (Δt 6/2) of the second, the third, and the fourth passes is 2.5 °C/s, 2.6 °C/s, and 2.7 °C/s, respectively. With the application of cooling, the hardness distribution shows a 455 HV hardness value at 13 mm from the center of welded metal with a value of 455 HV, i.e., which satisfy the requirements of military standards (Fig. 18, "Hardness distribution results").

Visual, PT, and RT testing show crack-free welded joints without any defects. This indicated that the gentle cooling by compressed air after each pass with a pressure of 6 bars did not show any cracks and it is safe.

Joint configuration and dilution percentage

Figure 10 shows the dilution percentages of the single V and single bevel groove joints with the GTAW process using both AWS A5.18 ER70S-6 and AWS A5.9 ER 307 filler wires. The dilution in the single V joint was less than in the single bevel joint using two types of filler metals. The dilution greatly affects the mechanical and metallurgical properties of weld metal that deviate from the pure filler wire properties. This can be observed in the tensile strength of welded joint shown in Table 9 ("Tensile strength"), and the microstructure of weld metal is shown in Figs. 25 and 26 ("SEM characterization of welded joints"). The existence of martensite structure greatly affects the improvement of tensile strength. This can be explained using the Schaeffler diagram [40]. The same results were obtained in the study of Sun Y. L. et al. [41].

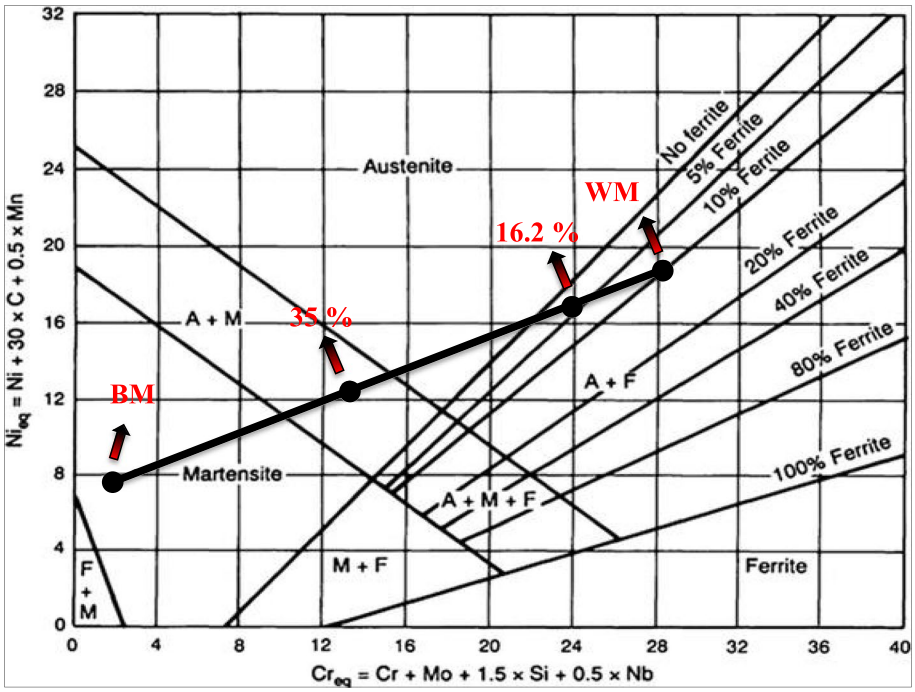

Fig. 11 Schaeffler diagram indicating the locations of pure weld metal (WM), base metal (BM), and the compositions of weld metal with different joints (different dilutions)

They discovered that the dilution in multi-pass steel welds using GTAW and SAW processes increases in dilution that favors martensite formation. The joint configuration has a significant effect on the increment of dilution rather than the increase of heat input (using AWS A5.9 ER307 filler wire) as shown in Fig. 10.

Figure 11 shows the Schaeffler diagram indicating two different dilution levels using a single V groove (16.2% dilution) and single bevel groove (35% dilution) when applying AWS A 5.9 ER 307 as a filler metal. The figure indicates that the microstructure of the weld metal is mainly austenite and delta ferrite using a single V groove (16.2% dilution) and is mainly martensite and austenite using a single bevel groove (35 % dilution). This was confirmed with the microstructure observations shown in Figs. 22 and 23 and SEM observation shown in Fig. 26.

Mechanical properties of welded joints

Tensile strength

Table 9 and Fig. 12a show the results of the tensile strength of welded joints. The higher tensile strength was obtained using carbon steel and austenitic stainless steel filler wires with a single bevel groove. The dilution of weld metal causes a great increase in the tensile strength of welded joints. All the welded joints were fractured at the weld metal as shown in Fig. 12b; Aleksandar Cabrilo et al. [27] studied the welding of PROTAC 500 armor steel, and they could obtain a tensile strength of about 830 MPa when they left the specimens cooled in the air after each pass. However, cooling by compressed air resulted in a higher ultimate tensile strength (906 MPa).

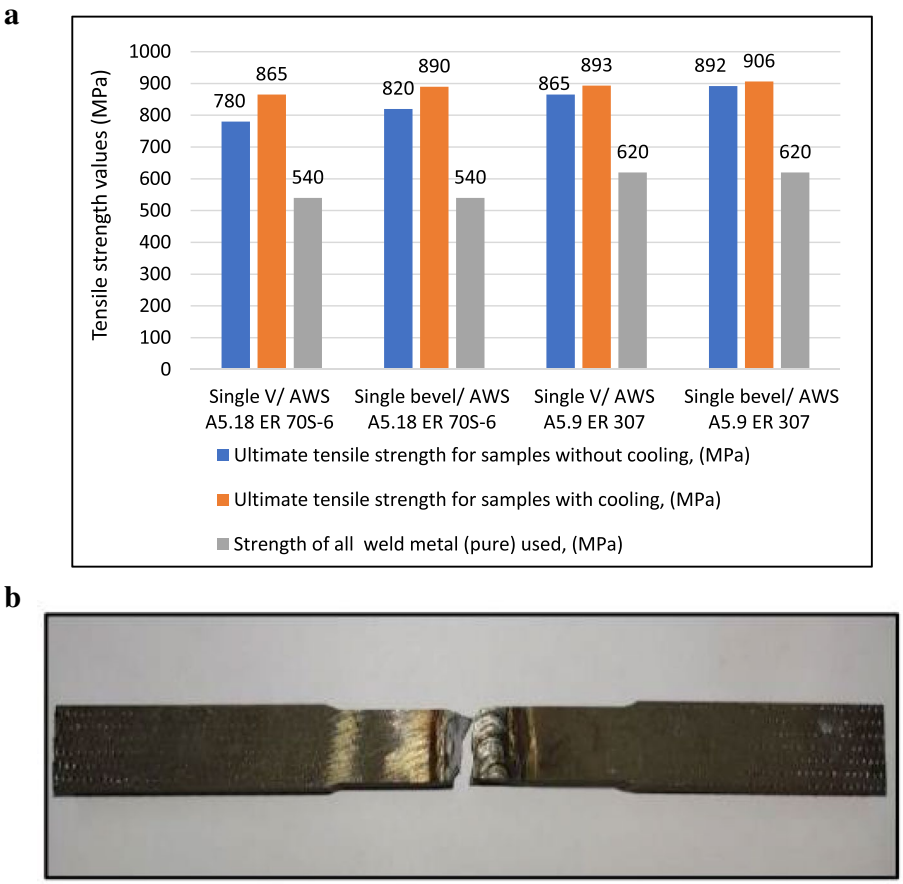

Fig. 12 **a** Tensile strength of welded joints. **b** Fracture location of the tensile test specimens

Table 10 Charpy V-notch impact properties of welded joints

Joint type and filler metal classification	Charpy V-notch impact test (CVN) results in (J)							
	WM at RT, without cooling	WM at −40 °C, without cooling	WM at RT, with cooling	WM at −40 °C, with cooling	HAZ at RT, with cooling	HAZ at −40 °C, with cooling	CVN of the used filler metal at RT [34]	CVN of the used filler metal at −40 °C [34]
Single V/AWS A 5.18 ER70S-6	101	42	119	50	100	83	120	50
Single bevel/ AWS A 5.18 ER70S-6	77	31	143	59	122	115	120	50
Single V/AWS A 5.9 ER307	131	60	157	65	115	108	120	110
Single bevel/ AWS A 5.9 ER307	86	52	147	61	125	104	120	110

Using a single bevel groove resulted in an increase in the ultimate tensile strength of the joint by about 5% more than using a single V-groove joint. However, using austenitic filler metal AWS A5.9 ER307 resulted in an increase in the joint strength by about 10% more than using carbon steel filler metal AWS A5.18 ER70S-6.

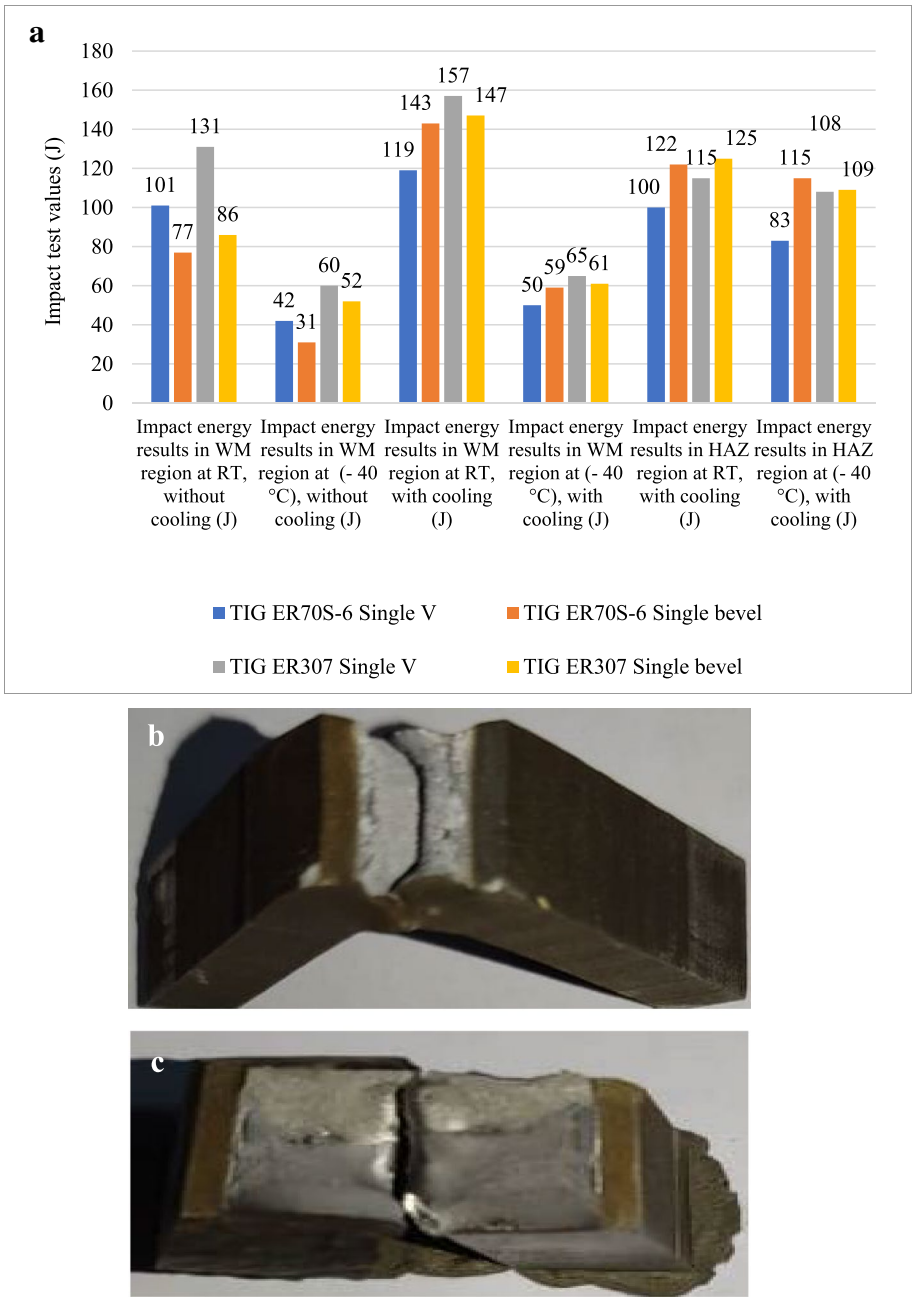

Fig. 13 **a** Charpy V-notch impact values of welded joints. **b** Fracture surface of the impact test where V-notch is at the welded metal. **c** Fracture surface of the impact test where V-notch is at HAZ

An application of cooling resulted in an increase in the joint strength which may reach to about 10%.

Charpy V-notch impact test results

Table 10 and Fig. 13a show the Charpy V-notch impact tests results that were conducted at room temperature and at −40 °C in the weld metal region. In addition, the test was

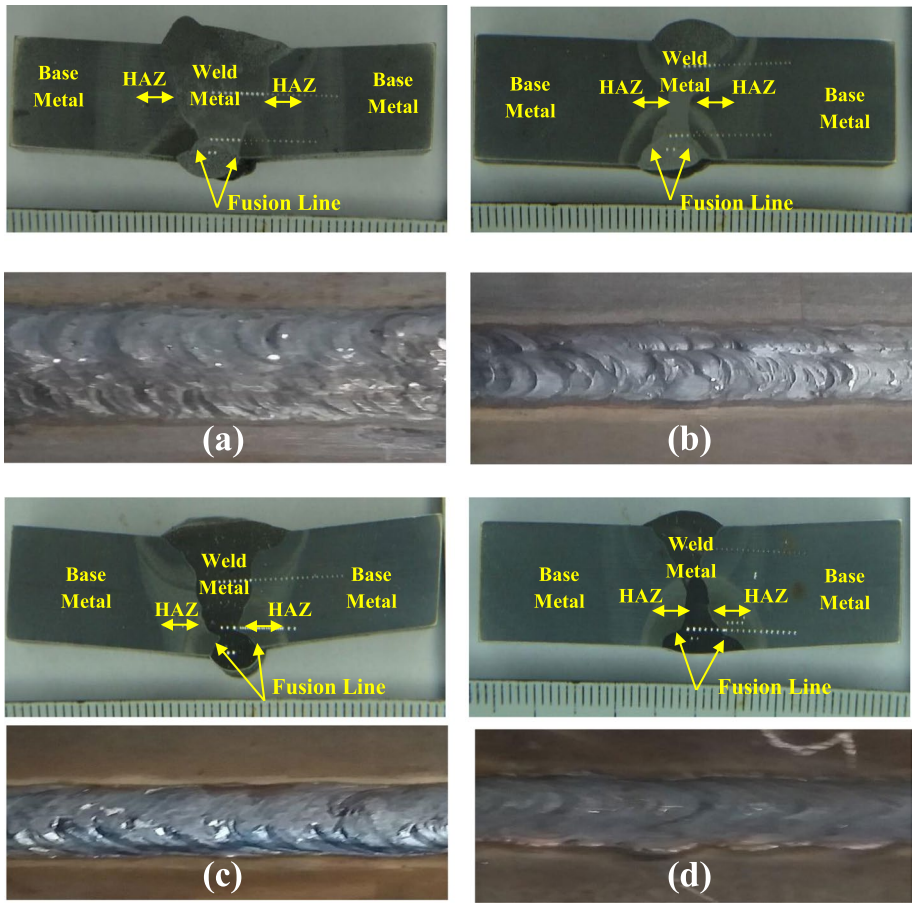

Fig. 14 Weld face of the final weld beads and macrography of welded sample. **a** Single V using AWS A 5.18 ER70S-6 with cooling. **b** Single bevel using AWS A 5.18 ER70S-6 with cooling. **c** Single V using AWS A5.9 ER307 with cooling. **d** Single bevel using AWS A 5.9 ER307 with cooling

performed in the heat-affected zone. These results show that the toughness energy values using austenitic weld metal are higher than that obtained using carbon steel. It can be noted that a single bevel groove for all specimens achieved the highest values for impact energy as shown in Fig. 13a and Table 10. All weld metal notched impact specimens were fractured at weld metals as shown in Fig. 13b. However, all HAZ notched impact specimens were fractured at HAZ as shown in Fig. 13c. The same results were obtained with Tekin Özdemir [42]. However, in our finding, the impact resistance results are higher than that of Tekin Özdemir's finding.

At room temperature, using a single V groove resulted in an increase in weld metal CVN impact strength to about 20% with carbon steel filler metal and to about more than 30% with an austenitic filler metal.

Welded joint shapes using different wires and their joint configurations

The welded joints are all homogenous without the occurrence of defects, inclusions, or cracks. Penetration of all weld passes is sufficient, and no lack of fusion was noticed in all

Table 11 Hardness distribution of the joint welded using AWS A5.18 ER70S-6 filler wire and applying a single V-groove joint

Position	**WM**											**HAZ + BM**						
Pitch (mm)	**1**	**1**	**1**	**1**	**1**	**1**	**1**	**1**	**1**	**1**	**1**	**1**	**1**	**1**	**1**	**1**	**1**	**1**
Distance (mm)	**0**	**1**	**2**	**3**	**4**	**5**	**6**	**7**	**8**	**9**	**10**	**11**	**12**	**13**	**14**	**15**	**16**	**17**
Center region for the welded sample with cooling	178	180	182	185	194	335	338	356	358	365	374	385	412	435	450	455	462	470
Root region for the welded sample with cooling	214	215	225	228	229	519	530	475	465	460	455	450	445	440	435	433	430	429
Center region for the welded sample without cooling	162	165	169	175	183	270	292	313	321	328	348	336	352	354	355	353	351	361

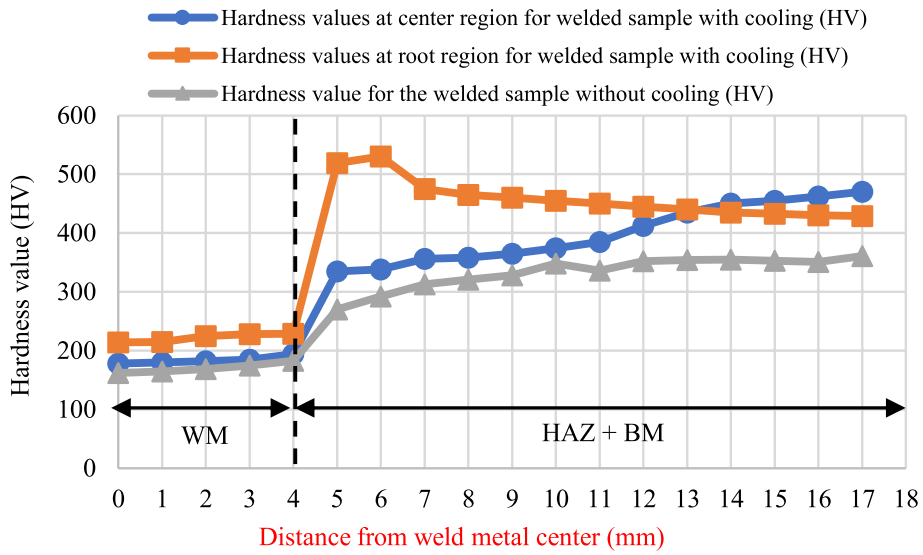

Fig. 15 Hardness distribution in the specimen welded using AWS A5.18 ER 70S-6 and joint a single V

samples. This was confirmed by a radiographic test for all the samples. All the samples were accepted. Also, a magnetic particle test (MT) was applied for specimens welded with ferritic filler wire and dye penetrant test (PT) is applied to the specimens welded with austenitic filler wire. No cracks were observed in all the specimens welded with or without the application of compressed air. Figure 14a, b, c, and d shows the welded joint weld faces and their macrostructures.

Hardness distribution results

Table 11 and Fig. 15 show the hardness distribution of the joint welded using AWS A5.18 ER70S-6 filler wire and applying a single V-groove joint. Without cooling, the hardness distribution at the mid-depth of the cross section of the specimen shows the lower base metal hardness values. The application of cooling resulted in the significant retainment of base metal hardness at a distance of 14 mm (450 HV) from the centerline of weld metal.

At the root, the application of cooling resulted in high weld metal hardness. This could be attributed to the higher dilution of weld metal from base metal and the high cooling rate.

In the previous papers [7], the plate thickness was 6 mm (SEWBOR 500), and the retained hardness was obtained at 15 mm without application of cooling. Aleksandar Cabrilo et al. [27] applied GMAW on an 11-mm-thick plate (PROTAC 500). The retainment of hardness was obtained at 14 mm from the centerline of weld metal. Cooling was not applied; however, the specimen was left to cool after each pass to about 150 °C (interpass temperature was 150 °C) [27]. Magudeeswarana V. G. et al. [16] used a 14-mm plate (AISI 4340) thickness with different welding processes and filler metals. Reduction of heat input to 1.33 kJ/mm resulted in the retainment of base metal hardness after about 13 mm [16].

Table 12 and Fig. 16 show the hardness distribution of the joint welded using AWS A5.18 ER70S-6 filler wire and applying a single bevel groove joint. Without cooling,

Table 12 Hardness distribution of the joint welded using AWS A5.18 ER70S-6 filler wire and applying a single bevel groove joint

Position	WM											HAZ + BM						
Pitch (mm)	1	1	1	1	1	1	1	1	1	1	1	1	1	1	1	1	1	1
Distance (mm)	0	1	2	3	4	5	6	7	8	9	10	11	12	13	14	15	16	17
Center region for the welded sample with cooling	203	204	215	229	275	356	347	382	403	407	410	425	439	455	460	465	475	480
Root region for the welded sample with cooling	240	247	248	263	263	404	475	492	494	495	508	511	512	517	523	525	520	521
Center region for the welded sample without cooling	183	188	188	189	194	342	358	395	413	442	443	359	375	365	372	364	370	370

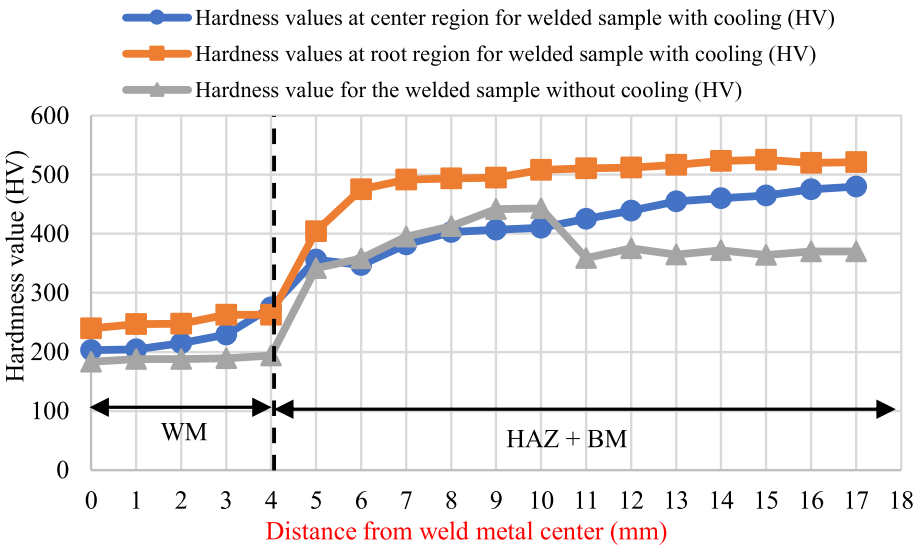

Fig. 16 Hardness distribution in the specimen welded using AWS A5.18 ER 70S-6 and joint a single bevel

the hardness distribution at the mid-depth of the cross section of the specimen shows a slight increase in the hardness values at the HAZ and an abrupt decrease in the values at the base metal. With cooling, the base metal hardness was retained at a distance of 13 mm (455 HV) from the weld metal center. This is attributed to higher dilution and higher cooling rates.

At the root, application of cooling resulted in a significant increase in the hardness values at the root that reaches to 510 HV at a distance of 7 mm from the weld metal centerline.

Our finding proves that the cooling by using gentle compressed air after each pass resulted in a retainment of base metal hardness after a distance of 7 mm at the root and at 13 mm at the mid-depth compared with the finding of Aleksandar Cabrilo et al. [27] and Magudeeswarana V. G. et al. [16].

Table 13 and Fig. 17 show the hardness distribution of the joint welded using AWS A5.9 ER 307 filler wire and applying a single V-groove joint. Without cooling, the hardness distribution at the mid-depth of the cross section of the specimen shows an increase in the hardness values without retainment of the base metal hardness at a distance less than 16 mm. With the application of cooling, the base metal hardness was retained at a distance of 15 mm (460 HV) from the weld metal center.

At the root, the application of cooling resulted in the high hardness values at the root and the retainment of base metal hardness at a distance of 4 mm (473 HV) from the weld metal centerline. This could be attributed to the higher cooling rates and the high dilution of weld metal.

In the previous paper [7], the retainment of hardness value at 16 mm without cooling could be attributed to the low heat input (about 0.8 kJ/mm) applied to 6-mm thick plate compared with 1.3 kJ/mm in this research work applied to 10-mm-thick plate. The application of compressed air is beneficial to compensate for the high heat input applied in this thick plate (10 mm).

Table 13 Hardness distribution of the joint welded using AWS A5.9 ER 307 filler wire and applying a single V-groove joint

Position	**WM**											**HAZ + BM**						
Pitch (mm)	**1**	**1**	**1**	**1**	**1**	**1**	**1**	**1**	**1**	**1**	**1**	**1**	**1**	**1**	**1**	**1**	**1**	**1**
Distance (mm)	**0**	**1**	**2**	**3**	**4**	**5**	**6**	**7**	**8**	**9**	**10**	**11**	**12**	**13**	**14**	**15**	**16**	**17**
Center region for the welded sample with cooling	235	236	237	240	262	334	347	357	298	376	385	420	345	439	445	460	476	478
Root region for the welded sample with cooling	422	423	425	471	473	535	522	524	518	527	527	526	521	529	537	538	534	535
Center region for the welded sample without cooling	198	201	203	205	206	285	304	307	324	330	319	325	339	340	355	366	372	389

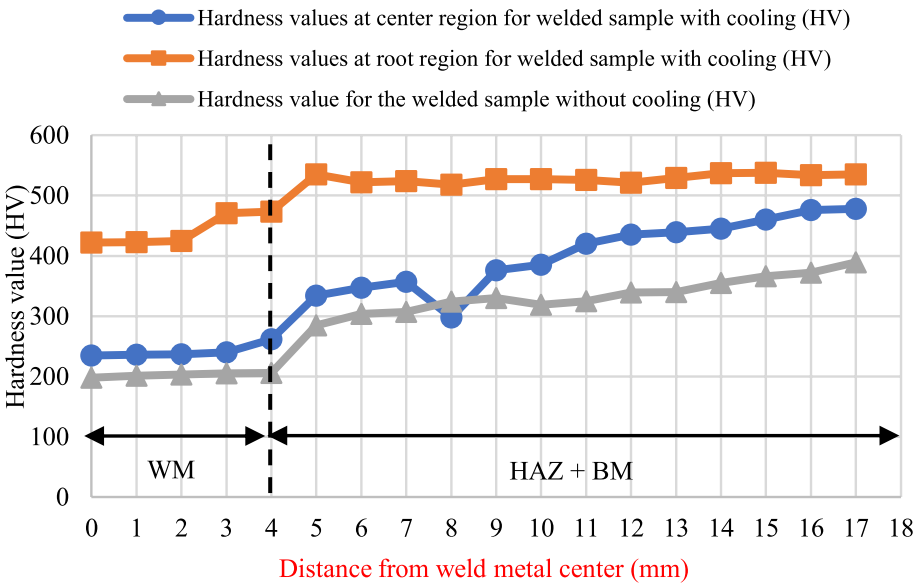

Fig. 17 Hardness distribution in the specimen welded using AWS A5.9 ER307 and joint a single V

Table 14 and Fig. 18 show the hardness distribution of the joint welded using AWS A5.9 ER 307 filler wire and applying a single bevel groove joint. Without cooling, the hardness distribution at the mid-depth of the cross section of the specimen shows an increase in the hardness values that occurred in the HAZ with a sudden decrease in the hardness at the base metal region. Application of cooling resulted in the significant retainment of base metal hardness at a distance of 13 mm (455 HV) from the centerline of weld metal.

At the root, the application of cooling resulted in a significant increase in the hardness values at the root that reaches to 522 HV at a distance of 5 mm from the weld metal centerline.

The application of cooling is necessary because trying to decrease the heat input to a lower value in the welding of this 10-mm-thick plate failed. Increase of heat input to about 1.4 kJ/mm and application of compressed air resulted in the success of the welding procedure and attainment of the base metal hardness value at a distance of 13 mm. The low heat input applied in welding of 6-mm-thick plate [7] resulted in the success of welding procedure without cooling by any means such as compressed air.

The same results were obtained by DAVID ROBLEDO et al. [18]. The increase in the rate of cooling was conducted by applying copper backing using GMAW process with a heat input of about 1 kJ/mm. This resulted in a reduction in the heat-affected zone and retainment of base metal hardness at a distance of about 9 mm from the center of the weldment.

Table 14 Hardness distribution of the joint welded using AWS A5.9 ER 307 filler wire and applying a single bevel groove joint

Position	WM											HAZ + BM						
Pitch (mm)	1	1	1	1	1	1	1	1	1	1	1	1	1	1	1	1	1	1
Distance (mm)	0	1	2	3	4	5	6	7	8	9	10	11	12	13	14	15	16	17
Center region for the welded sample with cooling	208	214	216	220	272	345	350	354	375	385	395	410	439	455	465	470	475	489
Root region for the welded sample with cooling	297	386	408	407	408	522	518	523	538	532	535	525	535	536	525	526	544	547
Center region for the welded sample without cooling	179	182	187	191	242	405	450	440	468	459	445	395	400	387	405	398	356	340

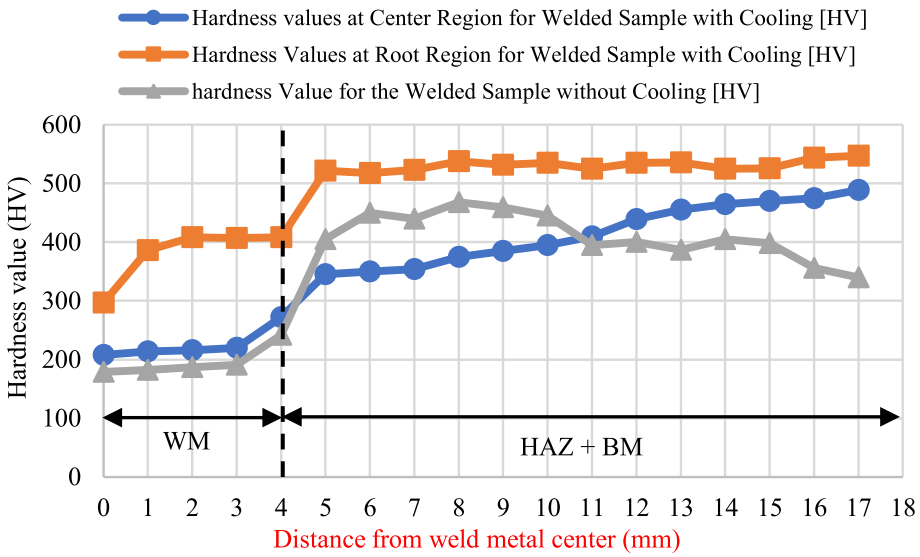

Fig. 18 Hardness distribution in the specimen welded using AWS A5.9 ER307 and joint a single bevel

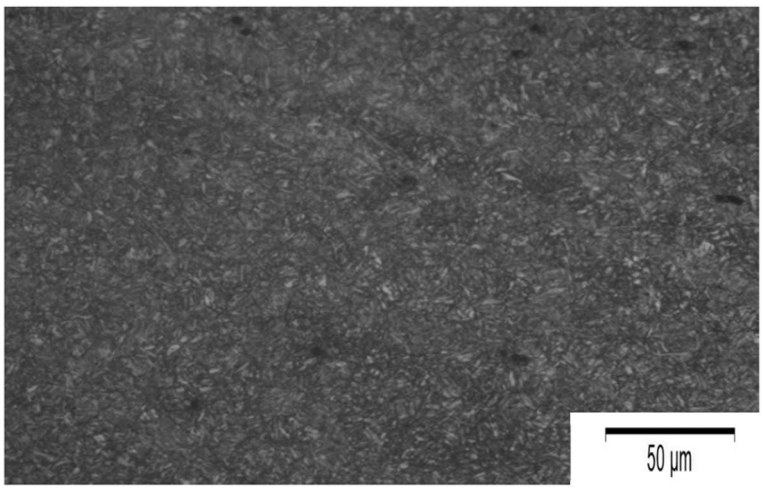

Fig. 19 The microstructure of the base metal (Armox 500T) armor steel

Microstructure analysis of welded joints

Figure 19 shows the microstructure of the base metal. It is tempered martensite with retained austenite.

Figure 20a and b shows the microstructure of the weld metal at the upper pass using carbon steel wire in the single V-joint groove with the cooling application. It is a columnar structure with ferrite and pearlite with coarse grain. However, at the root pass, the microstructure is a cellular structure with a bainitic structure as shown in Fig. 20b. Figure 20c shows the existence of an over-tempered

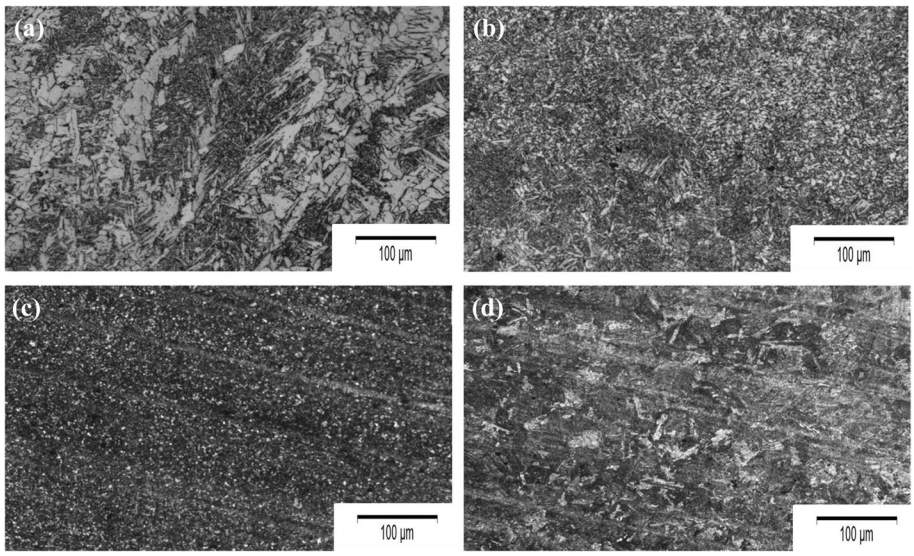

Fig. 20 Microstructure of single V welded joint using AWS A 5.18 ER70S-6 filler metal. **a** Weld metal. **b** The cellular structure with a bainitic structure in weld metal. **c** Over-tempering (softening zone) in HAZ zone. **d** Martensite structure in HAZ zone

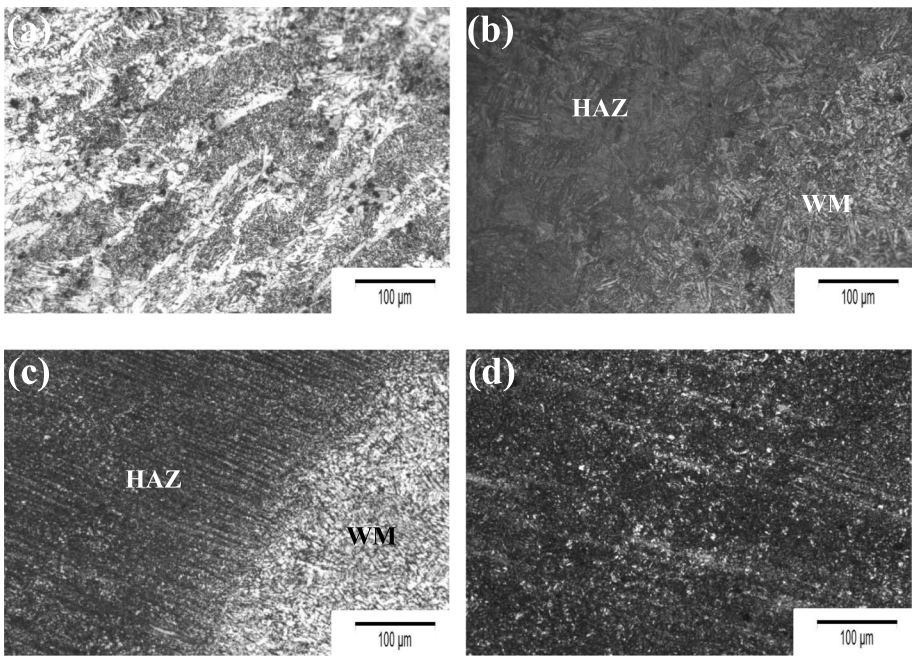

Fig. 21 Microstructure of single bevel welded joint using AWS A 5.18 ER70S-6 filler metal. **a** Weld metal. **b** Weld metal at the root pass and HAZ region. **c** Weld metal zone at the upper pass and HAZ region. **d** Over-tempering (softening zone) in HAZ zone

microstructure, and that indicated the rise of this region's temperature to a high value lower than the austenitizing temperature yet over-tempering temperature. Figure 20d shows also the existence of the martensite structure in the HAZ, which

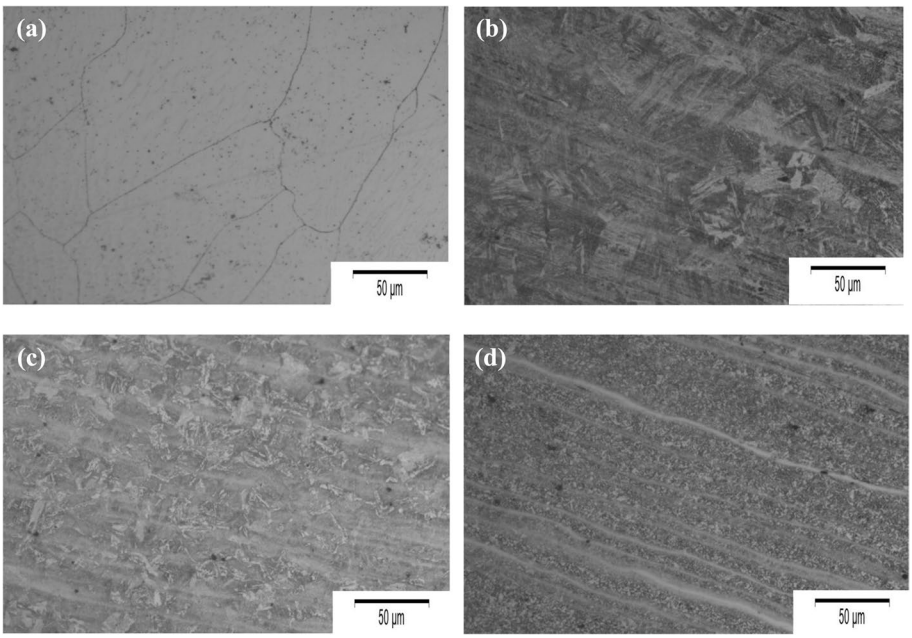

Fig. 22 Microstructure of single V welded joint using AWS A 5.9 ER 307 filler metal. **a** Weld metal. **b** Martensite structure in weld metal zone. **c** Grain coarsening martensite structure in HAZ zone. **d** Over-tempering (softening zone) in HAZ zone

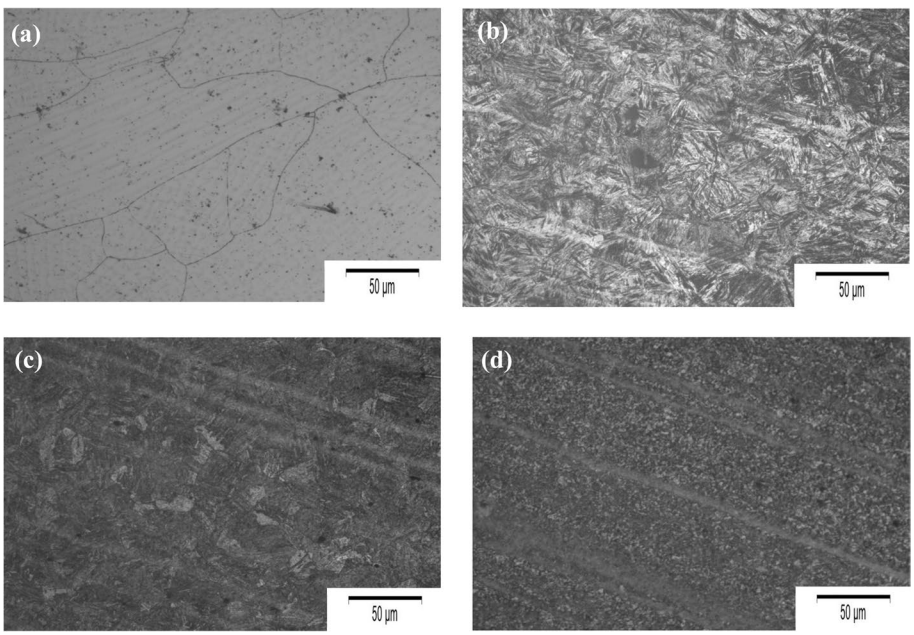

Fig. 23 Microstructure of single bevel welded joint using AWS A 5.9 ER 307 filler metal **a** Weld metal. **b** Martensite structure in weld metal zone. **c** Grain coarsening zone containing a martensitic structure in HAZ zone. **d** Over-tempering (softening zone) in HAZ zone

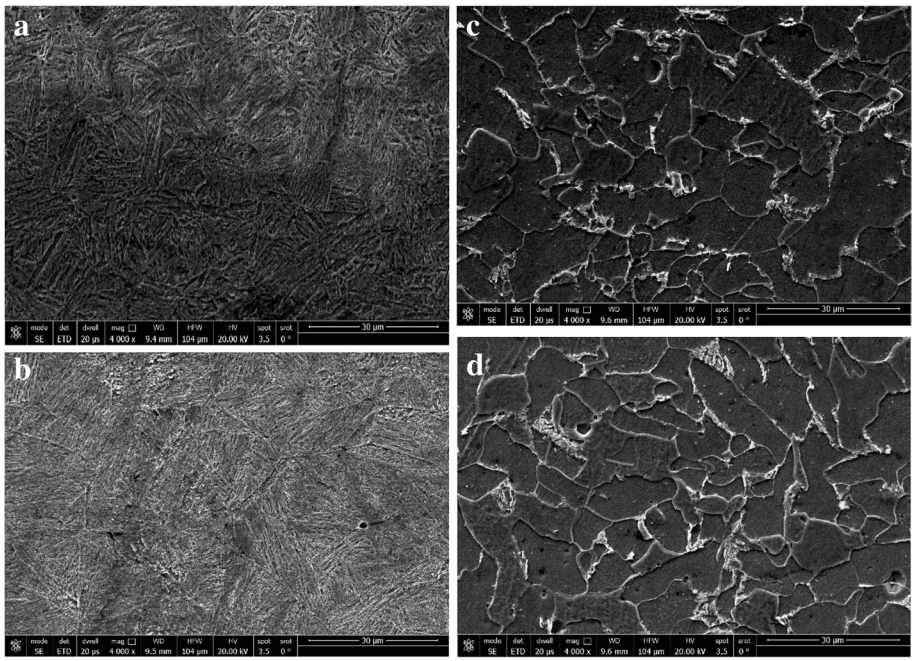

Fig. 24 SEM observations of single V welded joint using AWS A5.18 ER70S-6 filler metal. **a** Tempered martensite in base metal. **b** Grain refinement martensitic structure in HAZ zone. **c** and **d** Weld metal region composed of ferrite and pearlite

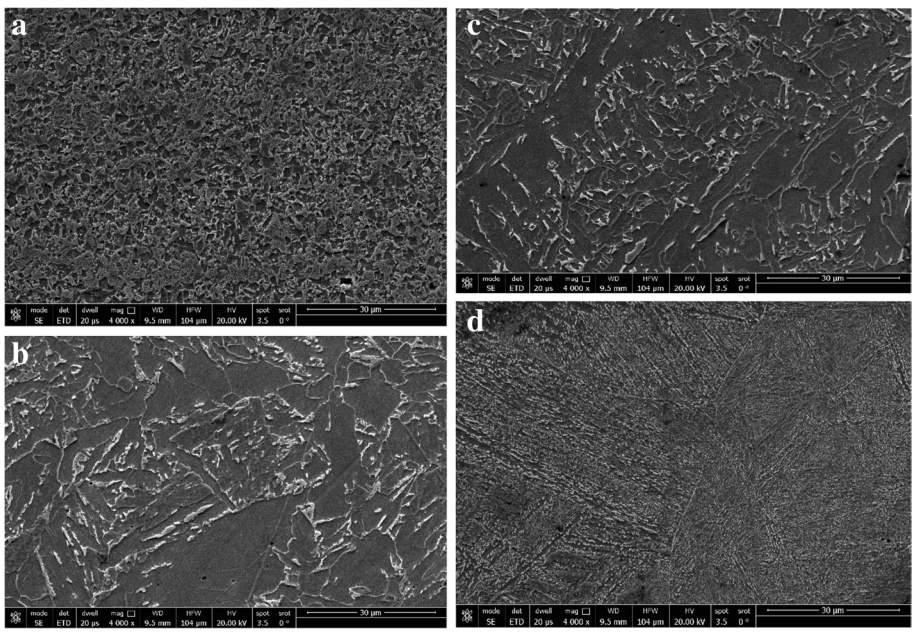

Fig. 25 SEM observations of single bevel welded joint using AWS A5.18 ER70S-6 filler metal. **a** Martensitic structure in HAZ zone, **b**, **c**, and **d** weld metal zone composed of columnar structure of ferrite and pearlite, and **d** martensite structure

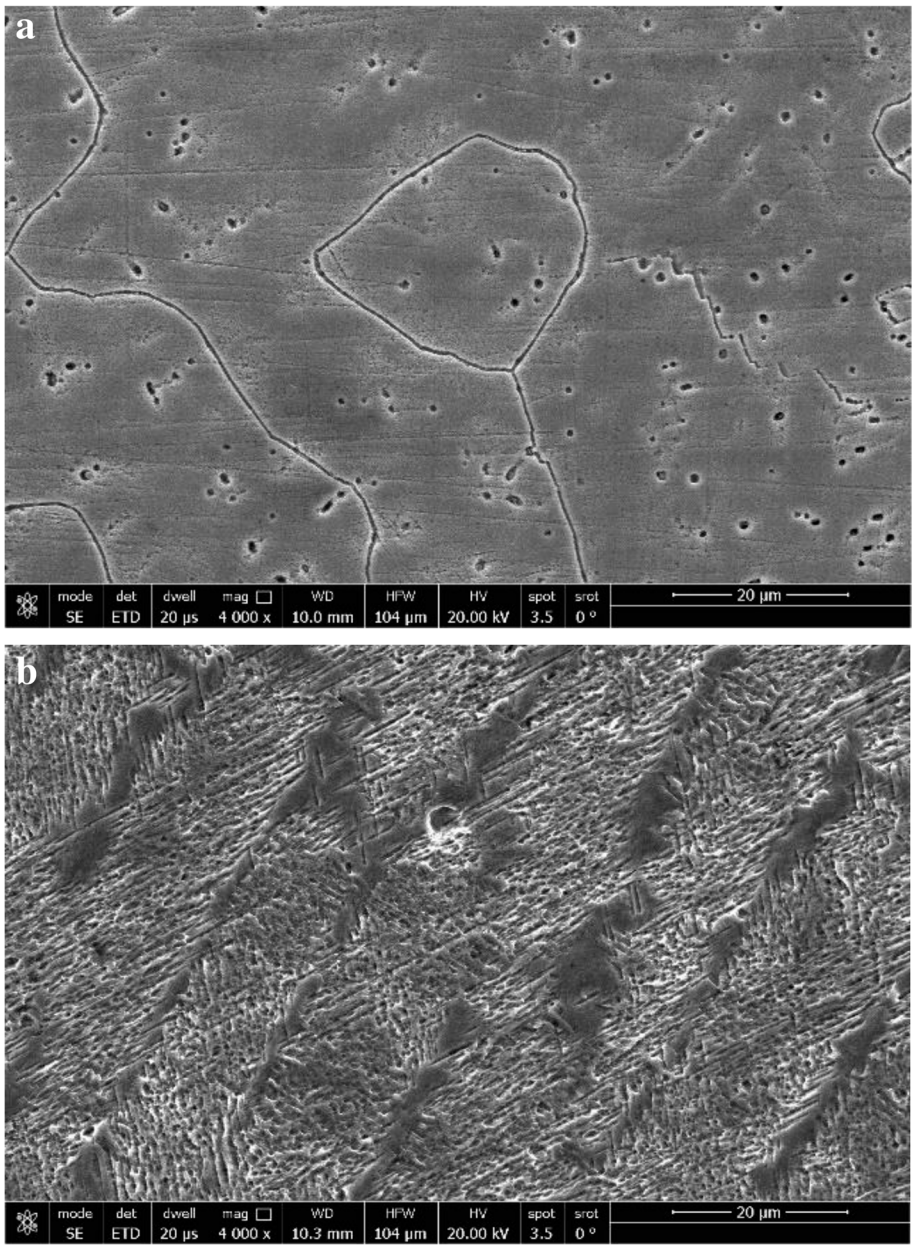

Fig. 26 SEM observations of single V and bevel welded joint using AWS A5.9 ER 307 filler metal. **a** The center of the weld metal with a single V groove with cooling. **b** Martensitic structure in the weld metal using single bevel groove with cooling at the center

indicates that this zone reached a temperature of about 1250 °C and cooled rapidly to form these phases.

Figure 21a shows the microstructure of the weld metal at the upper pass using carbon steel wire in a single bevel joint groove with the application of cooling. It is a columnar structure. Figure 21b shows the weld microstructure of the weld metal at the root pass. It is a bainitic structure with some acicular ferrite. Also, this figure shows microstructure at the HAZ in the root area. It is a martensitic structure. Figure 21c shows the weld metal and HAZ at the upper pass, the weld metal shows

the ferrite-pearlite structure, and the HAZ shows the over-tempered structure. Figure 21d shows the existence of over-tempering microstructure near the base metal zone, and this indicates the rise of this region's temperature to a high value lower than the austenitizing temperature yet over-tempering temperature.

Figure 22a shows the microstructure of the weld metal at the upper pass using AWS A5.9 ER 307 filler wire and a single V-joint groove with the application of cooling. It is an austenite structure. Figure 22b shows the existence of a martensitic microstructure in the area of weld metal too close to the base metal indicating the high percentage of dilution of the weld metal. Figure 22c shows the microstructure of the HAZ grain coarsening martensitic structure. The grain coarsening region reached a temperature of 1250 °C which causes grain coarsening. This was proven by the measuring of hardness in this region that reached 324 HV. Figure 22d shows the existence of an over-tempering microstructure in the HAZ.

Figure 23a and b shows the microstructure at the upper pass of the weld metal and heat-affected zone using a single bevel groove with the application of cooling. The weld metal at the center shows an austenitic structure with a hardness value of 272 HV as shown in Fig. 23a. Figure 22b shows the existence of a martensitic microstructure in the area of weld metal too close to the base metal indicated the high percentage of dilution of the weld metal. Figure 23c shows the microstructure at the HAZ in the grain coarsening zone containing a martensitic structure. Figure 23d shows the over-tempering zone (softening zone) in the HAZ.

In all specimens, the degree of softening of the HAZ depends of the weld thermal cycle, which is a function of heat input and cooling rate. This degree of softening in HAZ depends on the kinetics of phase transformation in welded steel [43, 44].

SEM characterization of welded joints

Figure 24 shows SEM observations of joint welded using AWS A5.18 ER70S-6 filler wire and applying a single V-groove joint with cooling. Figure 24a shows an SEM micrograph of the base metal which shows the tempered martensite structure. Figure 24b shows the micrograph of the HAZ. It is a martensitic structure. Figure 24c and d shows SEM micrographs of weld metal region that consists of ferrite and pearlite.

Figure 25 shows SEM observations of joint welded using AWS A5.18 ER70S-6 filler wire and applying a single bevel-groove joint with cooling. Figure 25a shows the micrograph of the HAZ that shows the over-tempered zone. Figure 25b and c shows SEM micrographs of weld metal region that consists of ferrite and pearlite. Figure 25d shows the weld metal too close to the base metal. It shows the martensitic structure. This was formed as a result of high dilution from base metal and the high cooling rate.

Figure 26a shows the microstructure at the center of the weld metal using AWS A5.9 ER307 filler wire with a single V groove with cooling. Figure 26b shows the microstructure of the weld metal close to the base metal using a single bevel groove with cooling. It is a martensitic structure that was formed as a result of high dilution and high cooling rate.

Conclusions

In this investigation, a detailed mechanical and metallurgical characterization was carried out on Armox 500T armor steel welded joints using the GTAW process, and the following results can be concluded.

1. Using AWS A5.18 ER70S-6 filler wire, both single V joint and single bevel joints passed the required tensile strength by the military standard. Also, the joints successfully regained the base metal hardness (about 450 HV) at a distance of 14 mm and 13 mm respectively from the center of weld metal.
2. Using AWS A5.9 ER307 filler wire, both single V joint and single bevel joints passed the required tensile strength by the military standard. Both successfully regained the base metal hardness (about 455 HV) at a distance of 15 mm and 13 mm respectively from the center of weld metal.
3. The ultimate tensile strength of joints welded using a single bevel is 906 MPa which is higher than that of joints welded using a single V groove is 865 MPa. This could be attributed to the increase in dilution percentage in the single bevel joints.
4. Both single V joint and single bevel joints passed the required Charpy V-notch impact test whether using carbon or stainless-steel wires.
5. The effect of heat input and cooling rate on the mechanical and microstructure of welded joints was studied. Reduction of heat input caused the narrow HAZ with a small reduction in its hardness values with less softening of its microstructure.
6. Using a single bevel groove with an austenitic steel filler metal, the weld metal at the area close to the base metal shows the formation of martensitic/austenitic microstructure as shown by SEM observation and verified by Schaeffler diagram (35% dilution).

Abbreviations

CVN	Charpy V-notch
Δt 8/5	The difference in temperature between 800 and 500 °C
Δt 6/2	The difference in temperature between 600 and 200 °C
SEM	Scanning electron microscope
PT	Dye penetrant testing
RT	Radiographic testing
MT	Magnetic particle testing

Acknowledgements

We would like to thank the Welding and Nondestructive Testing Department Central Metallurgical Research Institute (CMRDI) for their great efforts during practical experiments and tests. We would also like to thank the Faculty of Technology and Education, Production Technology Department, Helwan University for their interest in this study.

Authors' contributions

SMAA and MAM contributed to the experimental and theoretical work of this study. MAM and SMAA contributed to drafting this manuscript. SAA and KA contributed to drew its figures and its tables. Both authors contributed to revising this manuscript and its figures and its tables. The authors read and approved the final manuscript.

Funding

This study had no funding from any resource.

Availability of data and materials

All data generated or analyzed during this study are included in this published article.

Declarations

Competing interests

The authors declare that they have no competing interests.

Received: 5 March 2022 Accepted: 18 May 2022
Published online: 19 July 2022

References

1. Balakrishnan M, Balasubramanian V, Madhusudhan Reddy G (2013) Microstructural analysis of ballistic tests on welded armor steel joints. Metallogr Microstruct Anal 2(3):125–139
2. Jena PK, Mishra B, RameshBabu M, Babu A, Singh AK, Sivakumar K, Bhat B (2010) Effect of heat treatment on mechanical and ballistic properties of ahigh strength armour steel. Int J Impact Eng 37(3):242–249
3. Yurianto Y, Pratikto P, Soenoko R, Suprapto W (2019) TEMP effect of quench and temper on hardness and wear of HRP steel (armor steel candidate). East-Eur J Enterp Technol 3(12 (99)):55–61
4. Konca E (2020) A comparison of the ballistic performances of various microstructures in MIL-A-12560 armor steel. Metals 10(4):446
5. Arsić D, Nikolić R, Lazić V, Hadzima B, Aleksandrović S, Djordjević M (2014) Weldability estimates of some high strength steels. In: 42 International Conference "Zvaranie 2014", Tatranská Lomnica, Slovakia, pp 11–21
6. Popławski A, Kędzierski P, Morka A (2020) Identification of armox 500T steel failure properties in the modelling of perforation problems. Mater Des, Elsevier 190:108536
7. Morsy MA, El Hebeary R (2019) Weldability of armor steel. In: 72nd IIW Annual Assembly and International conference, 7-12 July 2019, pp 2–10
8. Grujicic M, Snipes JS, Galgalikar R, Ramaswami, S, Yavari R, Yen CF, Montgomery JS (2014) Improved gas metal arc welding multi-physics process model and its application to MIL A46100 armor-grade steel butt-welds. Multidiscipline Modeling in Materials and Structures
9. Lazić V, Arsić D, Nikolić RR, Djordjević D, Prokić-Cvetković R, Popović O (2017) Application of the high strength steel HARDOX 450 for manufacturing of assemblies in the military industry. Key Eng Mater 755:96–105
10. Arsić D (2013) Estimation of weldability and selection of optimal technology for welding of high strength steel class S690QL, master thesis. Faculty of Engineering in Kragujevac, Kragujevac (In Serbian)
11. Arsić D et al Selecting the optimal welding technology of high strength steel of the S690QL class. In: 19th International seminar of Ph.D. students, 29-31 January, Žilina, Slovakia, pp 5–9
12. Lazić V et al (2012) Estimates of weldability and selection of the optimal procedure and technology for welding of high strength steels, Steel Structures and Bridges 2012. Procedia Eng 40:310–315
13. Arsić D et al (2014) Application of high strength steels to responsible welded structures on motor vehicles. In: International Congress Motor Vehicles & Motors 2014, 9-10, Kragujevac, Serbia
14. Larsson TB, Berglund T (1992) Handbook on WELDING of Oxelösund steels. Steel plant SSAB Oxelösund, Sweden
15. Naveen Kumar S, Balasubramanian V, Malarvizhi S, Hafeezur Rahman A, Balaguru, V (2022). Effect of Welding Consumables on the Ballistic Performance of Shielded Metal Arc Welded Dissimilar Armor Steel Joints. J Mater Eng Perform 31(1):162–179
16. Magudeeswarana VG, Balasubramanianb G, Reddy M (2018) Metallurgical characteristics of armour steel welded joints used for combat vehicle construction. Def Technol 14(5):590–606
17. Maweja K, Stumpf W (2008) The design of advanced performance high strength low-carbon martensitic armor steels: microstructural considerations. Mater Sci Eng 480:160–166
18. Robledo DM, Gómez JAS, Barrada JEG (2011) Development of a welding procedure for mil a 46100 armor steel joints using gas metal arc welding. Dyna 78(168):65–71.
19. (2005) SSAB Armox welding recommendation. SSAB OxelOsund AB, OxelOsund
20. Madhusudhan Reddy G, Mohandas T, Sarma DS (2003) Cold cracking studies on low alloy steel weldments: effect of filler metal composition. Sci Technol Weld Join 8(6):407–414
21. Alkemade SJ (1996) The Weld Cracking Susceptibility of High Hardness Armour Steel. Defence Science and Technology Organization Canberra (Australia)
22. Saxena A, Dwivedi SP, Sharma S, Srivastava VS (2021) A comparative numerical analysis on the effect of welding consumables on the ballistic resistance of SMAW joints of armor steel. Appl Sci 2021(11):3629
23. Reddy GM, Mohandas T (1996) Ballistic performance of high-strength low-alloy steel weldments. J Mater Process Technol 57:23–30
24. Rathod DW (2021) Comprehensive analysis of gas tungsten arc welding technique for Ni-base weld overlay. In: Advanced welding and deforming, pp 105–126
25. Moinuddin SQ, Kapil A, Kohama K, Sharma A (2016) On process-structure -property interconnection in anti-phase synchronized twin-wire GMAW of low carbon steel. Sci Technol Weld Join 21:452–459
26. Abbasi K, Allam S, Khan MM (2012) An experimental study on the TEMP effect of MIG welding parameters on weld bead shape characteristics. IRACST – Eng Sci Technol 2:599–602
27. Cabrilo A, Geric K (2018) Fracture mechanic and charpy impact properties of a crack in weld metal, HAZ and base metal of welded armor steel. Procedia Structural Integrity 13:2059–2064
28. DEPARTMENT OF DEFENSE (1979) MIL STD 1185. Military Standard. Welding, high hardness armor, DoD
29. American Welding Society (1994) Structural Welding Committee, American Welding Society, and American National Standards Institute. Structural Welding Code--steel. Amer Welding Society
30. AMERICAN WELDING SOCIETY (2002) D1.1 Structural welding code- steel. AWS, pp 119–179
31. AMERICAN SOCIETY FOR MECHANICAL ENGINEERS (1998) ASME boiler and pressure vessel code. Section IX welding and brazing qualifications. ASME, pp 12–47
32. SSAB OXELOSUND SWEDEN (2008) The steel book, Sweden [online 10.6.2012]. Available: http://www.ssab.com
33. Krishna Murthy N, Janaki Ram GD, Murty BS, Reddy GM, Rao TJP (2014) Carbide-free bainitic weld metal: a new concept in welding of armor steels. Metall Mater Trans B 45:2327–2337
34. Voestalpine (2019) Böhler of welding product catalogue, pp 30–360

35. ESAB (2016) Welding filler metal. In: Databook
36. Nanavati PK (2020) Importance of dilution in dissimilar metal welding and calculations of weld metal compositions. Weld Knowl
37. American Society for Testing and Materials. Standard test method for Knoop and Vickers hardness of materials, ASTM E384-11. 2011.
38. American Society for Testing and Materials. Standard test methods and definitions for mechanical testing of steel products, ASTM A370-14. 2014.
39. American Society for Testing and Materials. Standard test methods for notched bar impact testing of metallic materials, ASTM, E23-1a. 2002.
40. Schaeffler AL (1949) Constitution diagram for stainless steel weld metal. Metal Prog 56(11):680–680B
41. Sun YL, Obasi G, Hamelin CJ, Vasileiou AN, Flint TF, Balakrishnan J, Smith MC, Francis JA (2019) Effects of dilution on alloy content and microstructure in multi-pass steel welds. J Mater Process Technol 265(March 2019):71–86
42. Özdemir T (2020) Mechanical & microstructural analysis of armor steel welded joints. Int J Eng Res Dev 12(1):166–175
43. Ji HK, Oh YJ, Soon Hwang II, Kim DJ, Kim JT (2001) Fracture behavior of heat-affected zone in low alloy steels. J Nul Mat 299(2001):132–139
44. Wojnowski D, Oh YK, Indacochea JE (2000) Metallurgical assessment of the softened HAZ region during multipass welding. J Mfg Sci Eng (ASME) 122(2):310–315
45. Kim J-H, Choi S-W, Park D-H, Lee J-M (2015) Charpy impact properties of stainless-steel weldment in liquefied natural gas pipelines: effect of low temperatures. Mater Des 65(January 2015):914–922

Publisher's Note

Springer Nature remains neutral with regard to jurisdictional claims in published maps and institutional affiliations.

Submit your manuscript to a SpringerOpen journal and benefit from:

- ► Convenient online submission
- ► Rigorous peer review
- ► Open access: articles freely available online
- ► High visibility within the field
- ► Retaining the copyright to your article

Submit your next manuscript at ► springeropen.com